Journal of *Marine Science and Engineering*

MDPI

Article

Numerical Investigation on the Static Lateral Bearing Capacity and Failure Mechanism of Pile–Bucket Foundation

Mohamed A. Frah [1,2], Meijuan Xu [1,3], Lichen Li [1,4], Wenbing Wu [1,3,*], Maha A. Abusogi [5], Tasneem Idris [2], Jingliang Ye [1,6], Chunbin Wan [1,6] and Ruqin Luo [1,6]

1 Department of Civil Engineering, Faculty of Engineering, China University of Geosciences, Wuhan 430074, China; mohamedfrah239@gmail.com (M.A.F.); xumeijuannj@163.com (M.X.); 20121003645@cug.edu.cn (L.L.); xyni_cug@163.com (J.Y.); wangrb84@163.com (C.W.); 15172366829@139.com (R.L.)
2 Department of Civil Engineering, Faculty of Engineering and Technical Studies, University of Kordofan, El-Obeid 51111, Sudan; tasneemidris76@outlook.com
3 Department of Civil Engineering, Zhejiang University, Hangzhou 310027, China
4 Institute for Advanced Marine Research, China University of Geosciences, Guangzhou 511462, China
5 Department of Civil Engineering, Faculty of Engineering and Quantity Surveying, INTI International University, Nilai 71800, Malaysia; mahasoogy@hotmail.com
6 Wuhan Yucheng Construction Group Co., Ltd., Wuhan 430061, China
* Correspondence: zjuwwb1126@163.com

Abstract

The pile–bucket foundation, comprising a bucket attached to a single pile, represents an innovative offshore solution for supporting wind turbines. Previous studies on laterally loaded foundations have primarily focused on single piles and pile–bucket systems; however, the effects of bucket size and loading eccentricity on lateral capacity and soil failure mechanisms remain insufficiently understood. This study investigates the lateral performance of pile–bucket foundations in silty sand under static loading conditions. Seven three-dimensional numerical simulations were conducted to evaluate the influence of bucket diameter, embedment depth, and loading eccentricity. Results indicate that pile–bucket foundations achieve 37–60% higher lateral capacity than single piles and 3–4 times the capacity of standalone buckets. Increasing bucket diameter produces more significant improvements than increasing embedment depth, whereas higher loading eccentricity reduces lateral capacity, ranging from an 8% increase to a 10% decrease relative to a single pile. Increases in loading eccentricity, bucket diameter, and embedment depth shift the rotation center upward by approximately 3–9%, compared with a single pile. At the mudline, the bucket resists up to 75% of the lateral load, while the pile carries up to 92% of the moment. Failure mechanisms are dominated by excessive rotation, including wedge-type failure near the mudline and deep rotational soil flow. Increasing bucket diameter or embedment depth raises bending moments by 5–9%, while higher eccentricity amplifies them by 32–50%. A modified analytical formulation incorporating a correction factor of 1.16 improves the prediction of the rotation center position. These findings provide quantitative guidance for the design and optimization of pile–bucket foundations supporting offshore wind turbines.

Keywords: pile–bucket foundation; offshore wind turbines; lateral load-bearing capacity; static loading; failure mechanisms; bucket size; loading eccentricity; bending moment; rotation center

Check for updates

Academic Editor: Chungkuk Jin

Received: 10 February 2026
Revised: 1 March 2026
Accepted: 3 March 2026
Published: 5 March 2026

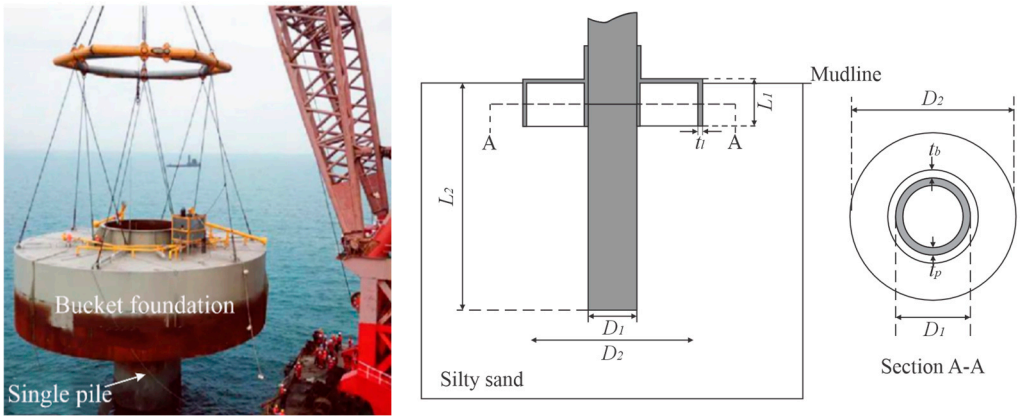
Copyright: © 2026 by the authors. Licensee MDPI, Basel, Switzerland. This article is an open access article distributed under the terms and conditions of the Creative Commons Attribution (CC BY) license.

1. Introduction

Onshore and offshore structures, including transmission towers, wind turbines, and floating platforms, are constantly exposed to lateral loads generated by wind, waves, and currents. The variable intensity of these loads has driven the design of pile foundations with different levels of stiffness. The stiffness of a pile, compared to the surrounding soil, is crucial in determining pile–soil interaction mechanisms [1].

Single-pile foundations are the most widely used solution for supporting offshore wind turbines (OWTs). As OWTs continue to increase in size, these foundations must provide increased capacity and stability. However, due to structural constraints, merely enlarging single piles leads to disproportionately higher construction and installation costs relative to the corresponding gains in loading capacity [2–5]. Therefore, refinement of single-pile foundation design is necessary to meet the requirements of next-generation OWTs.

Foundations play a critical role in supporting OWTs, directly influencing their structural integrity and long–term performance [6–9]. To accommodate varying environmental conditions, several foundation systems have been developed, including single piles, suction buckets, jackets, and floating platforms [10–14]. The performance of OWT foundations is largely governed by lateral loads and the resulting moments induced by wind, wave, and current actions [15–17]. In response to these challenges, a pile–bucket foundation was implemented at a wind farm in southeastern China in 2020 [18–21]. As shown in Figure 1, this composite foundation integrates a single pile with a bucket at the mudline, combining the pile's vertical bearing capacity with the enhanced lateral resistance provided by the bucket.



(**a**) (**b**)

Figure 1. Overview of the pile–bucket foundation system: (**a**) site photograph [19]; (**b**) schematic representation.

Bienen et al. [22] first proposed the pile–bucket foundation concept, introducing an innovative offshore foundation system. Using finite element analysis, they investigated its response under combined vertical, lateral, and moment loading and developed predictive functions for estimating its overall capacity.

Using large-scale model tests in soft marine clay, previous studies [18,23] investigated the static and cyclic lateral capacity of pile–bucket foundations and developed cyclic p–y relationships for the pile–bucket system. These studies demonstrated that the soil reaction mobilized by the bucket could reach up to 20 times that of a conventional single-pile foundation. More recent research has explored advancements in pile–bucket foundation design aimed at improving lateral resistance [24–28], including numerical and experimental investigations of cyclic behavior, grouted connections, and bearing mechanisms of pile–bucket systems [29–32].

Chen et al. [33] found that the pile–bucket system can effectively restrict rotation and displacement under dynamic loading. Foundation performance depends on factors such as soil type, geometric configuration, and loading conditions. For example, Pan et al. [34] investigated natural frequency variation in reinforced buckets, highlighting the requirement for structural reinforcement under variable loading.

Experimental and numerical investigations have further validated the potential of pile–bucket systems. Arshi et al. [35] performed 1 g model tests in cohesionless soil, showing that footing size, subsoil stiffness, and initial soil–footing contact significantly affect load transfer mechanisms. Building on these findings, incorporating skirts on pile footings has been shown to enhance lateral resistance. Comparative studies [35,36] highlight the advantages of composite foundations in reducing lateral loads and bending moments. Ma and Yang [36] reported that composite piles achieved a 10.7–19.5% reduction in bending moments. While suction buckets alone perform effectively under dynamic loading in deep water, they are less stable in shallow marine environments compared to single piles [37]. Liu et al. [38] demonstrated that combined vertical and lateral loading strongly influences lateral response. Zhang et al. [39] emphasized the role of soil properties and geometry, advocating the use of numerical simulations to optimize design parameters. Fan et al. [40] conducted experimental tests on skirted piles in saturated clay, confirming the significant effect of lateral mechanical behavior on overall foundation performance.

Recent studies have increasingly focused on pile–bucket offshore foundation systems that combine single piles and suction buckets, supported by large-scale model tests and advanced numerical simulations [29,30,41]. These investigations have improved understanding of lateral resistance mechanisms; however, most existing studies primarily evaluate global capacity or displacement responses, while quantitative assessment of load–moment interaction and rotation characteristics remains limited. In particular, the effects of bucket size and loading eccentricity on pile–bucket foundation behavior have not yet been comprehensively examined.

The present study investigates the lateral performance of pile–bucket foundations in silty sand under static loading. Seven three-dimensional finite element models, incorporating different bucket sizes and loading eccentricities, were analyzed to assess the overall pile–soil interaction. The evaluation considers lateral load–displacement response, moment–rotation behavior, load- and moment-sharing ratios, rotation center positions, bending moment distributions, and soil failure mechanisms. This approach provides a quantitative understanding of the mechanical interactions governing pile–bucket foundations under lateral loading.

2. Numerical Modeling Approach

This section describes the numerical studies performed to evaluate the lateral capacity of pile–bucket foundations under static loading using the finite element software Abaqus (version 2022) [42].

2.1. Foundation Structural Modeling and Soil Characterization

The pile–bucket foundation system shown in Figure 1 consists of a single pile, characterized by diameter D_f, embedment depth L_1, and wall thickness t_p, together with a shallow, large-diameter bucket, defined by diameter D_2, embedment depth L_2, lid thickness t_l, and wall thickness t_b. Both the single-pile and the pile–bucket foundation system were modeled using 3D eight-node linear solid elements (C3D8R). The material properties adopted for the structural components are summarized in Table 1, while the geometric parameters used in the parametric analysis are listed in Table 2.

Table 1. Material properties pile–bucket foundation.

Type	Density (Kg/m^3)	Young's Modulus (N/m^2)	Poisson's Ratio
Pile–bucket foundation	7850	206×10^9	0.3

Table 2. Geometric details of the pile–bucket foundation.

Type	D_1 (m)	L_1 (m)	D_2 (m)	L_2 (m)	t_p (mm)	t_l (mm)	t_b (mm)	e (m)
Model A	6	25	-	-	80	-	-	$1D_1$
Model B	-	-	15	3	-	100	100	$1D_1$
Model C	6	25	15	3	80	100	100	$1D_1$
Model D	6	25	20	3	80	100	100	$1D_1$
Model E	6	25	15	4.5	80	100	100	$1D_1$
Model F	6	25	15	3	80	100	100	$2D_1$
Model G	6	25	15	3	80	100	100	$3D_1$

A homogeneous, naturally consolidated silty sand was considered in this study. The soil behavior was modeled using the Mohr–Coulomb constitutive model, with the following parameter values: density 870 kg/m^3, Young's modulus 1.34×10^7 N/m^2, Poisson's ratio 0.3, cohesion 3.2×10^4 N/m^2, effective unit weight 10.2 kN/m^3, and an internal friction angle of 27°. These properties correspond to conditions commonly encountered in the offshore environment of Jiangsu Province, China [33].

The contact interaction between the pile–bucket foundation and the surrounding soil was modeled using hard contact in the normal direction, permitting separation and sliding between contacting surfaces. Tangential behavior was represented using a Coulomb friction model with a penalty-based formulation and a friction coefficient of 0.33 [4]. To focus on lateral bearing performance, the rotor–nacelle assembly, tower, and blades were simplified as a concentrated mass applied at the top of the foundation [33]. This modeling framework allows separation, sliding, and realistic load transfer at the soil–structure interface, ensuring that the simulation captures the nonlinear interaction behavior of the pile–bucket foundation under static lateral loading.

The Mohr–Coulomb model captures the fundamental strength-controlled mechanisms governing soil response under static lateral loading, including shear strength mobilization and overall yielding. While more advanced constitutive models (e.g., stress-dependent or hardening soil models) can better represent nonlinear stiffness and small-strain behavior, the Mohr–Coulomb model provides a balance between computational efficiency and physical representation. This approach is appropriate for the parametric analyses conducted to investigate lateral performance, load–moment sharing, rotation center evolution, and failure mechanisms of pile–bucket foundations.

2.2. Modeling Meshes

Owing to structural symmetry, only half of the foundation was modeled. Figure 2 illustrates the soil domain and representative finite element meshes adopted for the single-pile and pile–bucket foundation systems. The soil domain dimensions were initially defined as $10D_1$ in width for the single pile and $4D_2$ for the pile–bucket foundation. Regarding boundary conditions, a symmetry constraint was imposed along the model symmetry plane. The bottom boundary was fully restrained, whereas lateral displacements in both the x- and y-directions were restricted at the side boundaries. To improve computational efficiency and numerical accuracy, a refined finite element mesh was employed within the pile diameter and around the pile–bucket foundation, where stress gradients are expected to be highest, while a coarser mesh was used farther from the foundation.

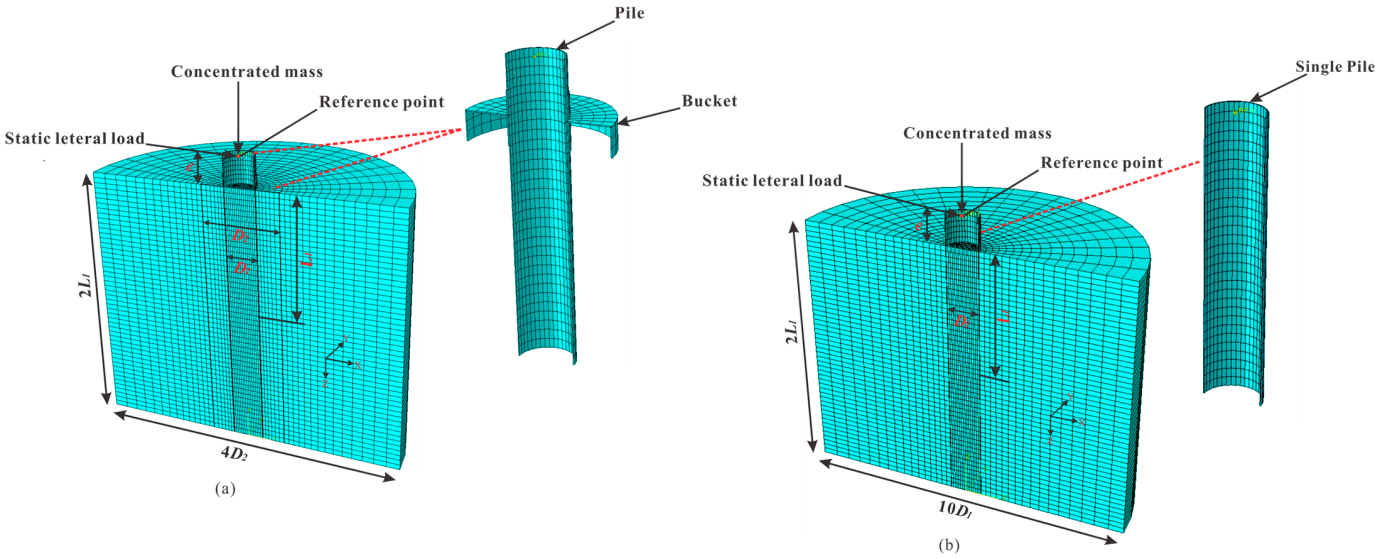


Figure 2. Finite element simulation model: (**a**) pile–bucket foundation, and (**b**) single-pile foundation.

A boundary sensitivity analysis was performed to evaluate the influence of soil domain size, as shown in Figure 3. Figure 3a presents the load–displacement responses of the pile–bucket foundation for soil domain diameters of $4D_2$ and $5D_2$, while Figure 3b shows the corresponding responses for the single pile with domain diameters of $10D_1$ and $11D_1$. For the pile–bucket foundation, increasing the domain diameter from $4D_2$ to $5D_2$ reduced the ultimate lateral capacity from 23,261.6 kN to 23,028.5 kN, corresponding to a difference of approximately 1.0%. Similarly, enlarging the single-pile domain from $10D_1$ to $11D_1$ changed the ultimate capacity from 17,200 kN to 17,121.6 kN, representing a difference of approximately 0.46%. In both cases, the load–displacement curves nearly coincide, indicating that the selected soil domain size is sufficient to minimize boundary effects. Therefore, the computed foundation response is not significantly influenced by the model boundaries.

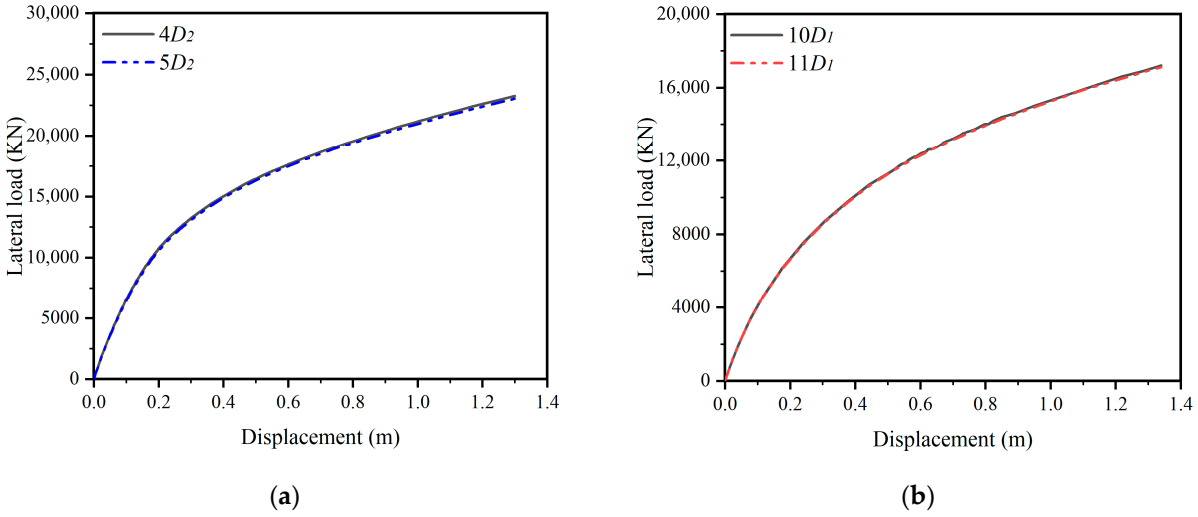


Figure 3. Sensitivity analysis of the FE model's boundary domain: (**a**) pile–bucket foundation, and (**b**) single-pile foundation.

2.3. Model Validation

To validate the numerical model, a finite element analysis was performed on a pile–bucket foundation without grout material or stiffeners. The results were compared with those reported by Chen et al. [33], whose model included grout material and stiffeners.

The moment (M) was obtained by applying a lateral displacement at a height (e) above the reference point. The resulting moment–rotation response predicted in this study was compared with the results of Chen et al. [33], as illustrated in Figure 4a. Good agreement was observed between the two studies, with a quantitative difference of approximately 1.8%. This small deviation can be attributed to the inclusion of grout material and stiffeners in the earlier study, which primarily affect the stiffness of the foundation system. In the present study, these components were not explicitly modeled because the focus was placed on soil–foundation interaction and overall lateral behavior. Overall, the comparison presented in Figure 4a confirms the accuracy and reliability of the adopted finite element modeling approach.

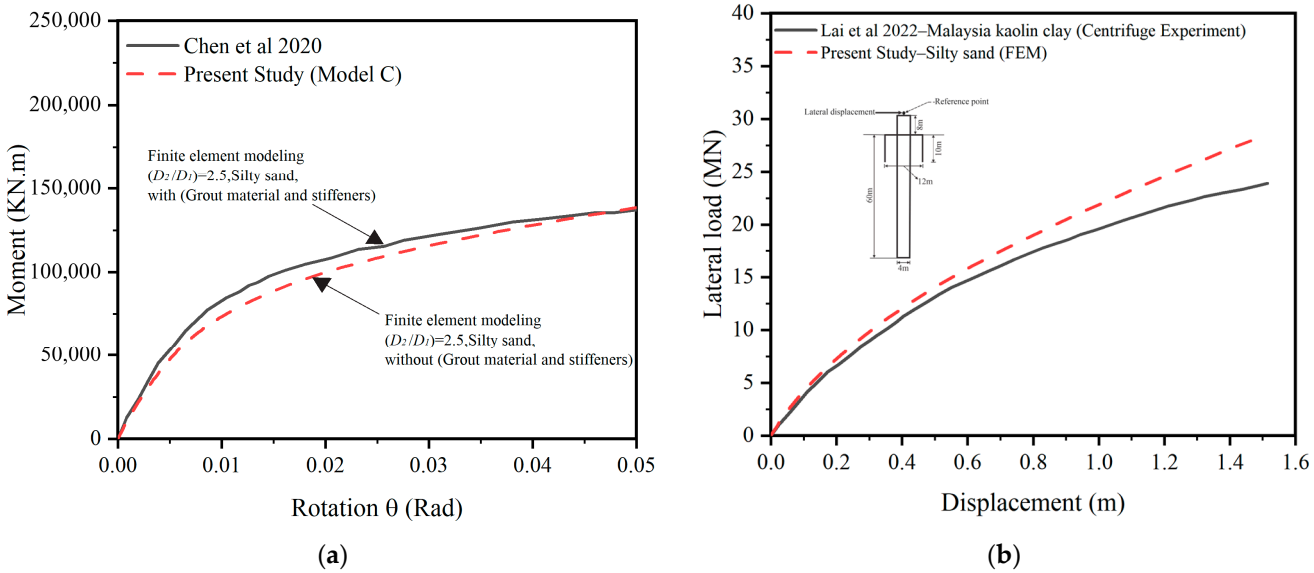


Figure 4. Comparison results: (**a**) finite element modeling [33], and (**b**) finite element modeling and centrifuge experiment [43].

To further verify the reliability of the numerical modeling approach, the predicted lateral load–displacement response was compared with the centrifuge test results reported by Lai et al. [43], as shown in Figure 4b, which investigated laterally loaded foundations in Malaysia kaolin clay. Although the soil type considered in the present study (silty sand) differs from the kaolin clay used in the centrifuge tests, the comparison focuses on overall behavioral trends and modeling methodology rather than reproducing identical soil properties. The numerical predictions successfully capture the nonlinear load–displacement response observed experimentally, including progressive stiffness degradation with increasing displacement. A quantitative comparison indicates a difference of approximately 18.8% between the predicted and experimental responses. The present model predicts slightly higher lateral resistance, which is reasonable given the higher shear strength and stiffness of silty sand compared with kaolin clay. The overall agreement in response trends supports the validity and robustness of the adopted finite element modeling strategy for analyzing laterally loaded pile–bucket foundations.

It is acknowledged that deviations between numerical predictions and experimental results may arise from multiple sources. Soil–pile–structure interaction is inherently complex, and finite element modeling involves uncertainties related to soil constitutive behavior, interface modeling, boundary conditions, mesh discretization, and parameter selection. Differences in soil type and mechanical properties between the present study and the experimental reference may also contribute to variations in the predicted response. In particular, although the Mohr–Coulomb model is widely adopted for static geotechnical

analysis, it may not fully capture stress-dependent stiffness, strain softening, or advanced nonlinear soil behavior. Interface assumptions between the pile, bucket, and surrounding soil introduce additional modeling simplifications. These challenges are consistent with broader issues in soil–pile–structure interaction modeling, as reviewed by Çetindemir [44]. Despite these inherent limitations, the numerical model successfully captures the overall nonlinear moment–rotation trend in Figure 4a and the load–displacement response in Figure 4b, supporting the robustness and reliability of the adopted modeling framework.

3. Static Load Performance in the Pile–Bucket Foundation System

This section investigates the static load response of the pile–bucket foundation system. Figure 5 illustrates the sign convention adopted for both loading and displacement. A vertical dead load (V), representing the self-weight of the wind turbine, was applied at a reference point located at the top of the foundation. In addition, a lateral displacement was imposed at an eccentricity (e) above this point until the foundation rotation reached 0.05 rad.

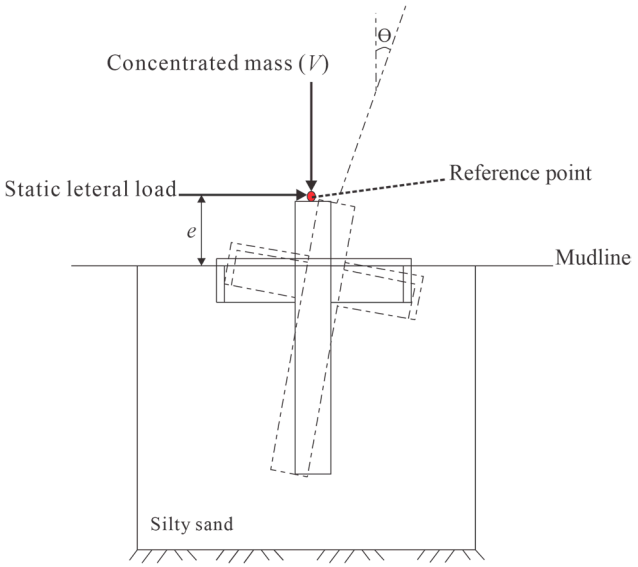


Figure 5. Schematic of the static loading setup.

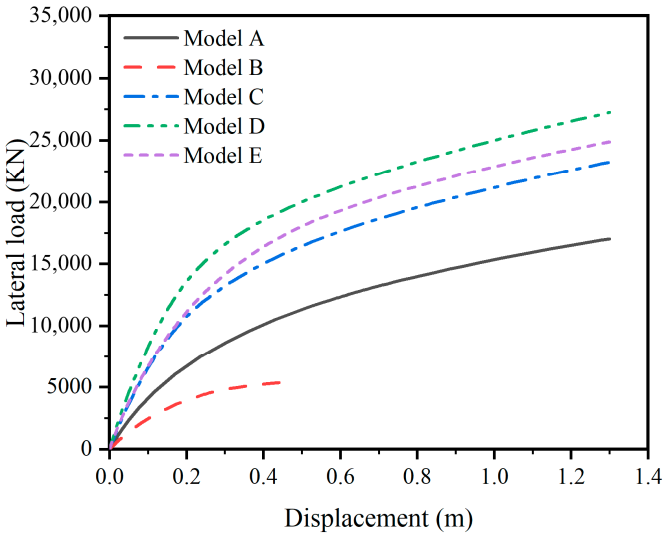
In this study, the ultimate lateral bearing capacity is defined as the lateral load corresponding to a foundation rotation of 0.05 rad, providing a consistent criterion for comparing different foundation configurations under displacement-controlled loading.

4. Results and Discussion

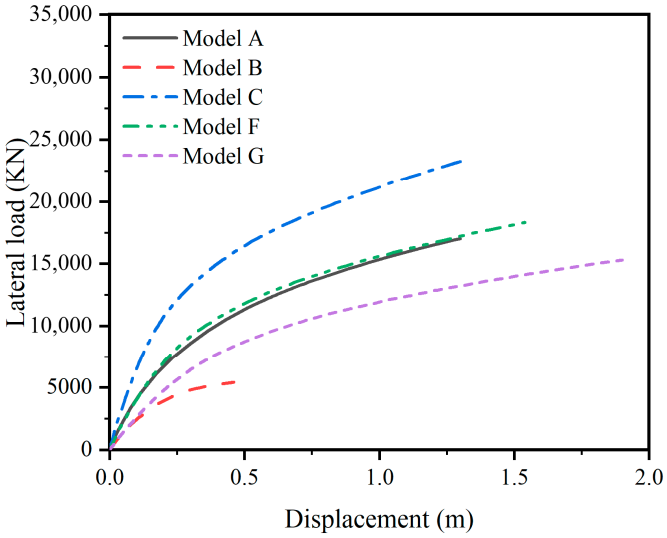
4.1. Lateral Bearing Capacity

Figure 6 presents the lateral load–displacement responses of pile–bucket foundations under different bucket sizes and loading eccentricities (e), where displacement corresponds to a rotation angle of 0.05 rad for each model. Figure 6a compares the lateral bearing capacities of a single pile, a standalone bucket, and a pile–bucket system. The pile–bucket foundation exhibits significantly higher lateral capacity than both the single pile and the standalone bucket, indicating strong interaction between the surrounding soil and the composite foundation compared with its individual components. Quantitatively, the results indicate that pile–bucket foundations achieve approximately 37–60% higher lateral capacity than single piles and 3–4 times the capacity of standalone buckets. Increasing bucket diameter results in a more pronounced improvement in both initial stiffness and lateral bearing capacity than increasing bucket embedment depth, demonstrating that

diameter plays a dominant role in enhancing lateral resistance. Figure 6b illustrates the effect of loading eccentricity on lateral bearing capacity. As eccentricity increases, both initial stiffness and lateral capacity decrease progressively, with the response ranging from an approximately 8% increase to a 10% reduction relative to the single-pile case. These trends are consistent with previously reported finite element analyses and experimental observations [33,45].



(**a**)

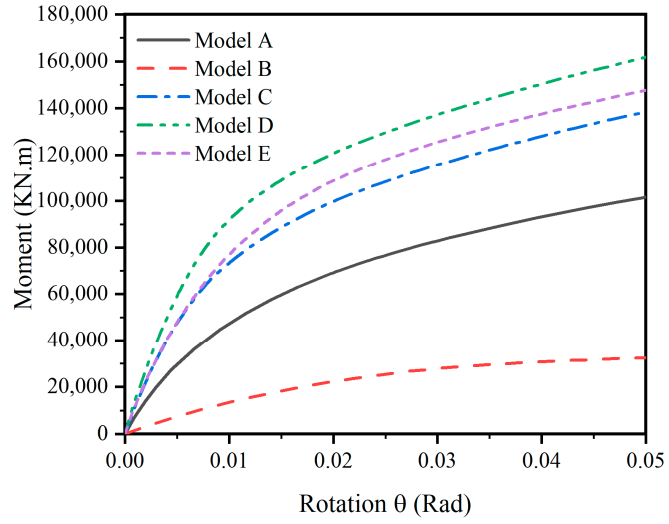


(**b**)

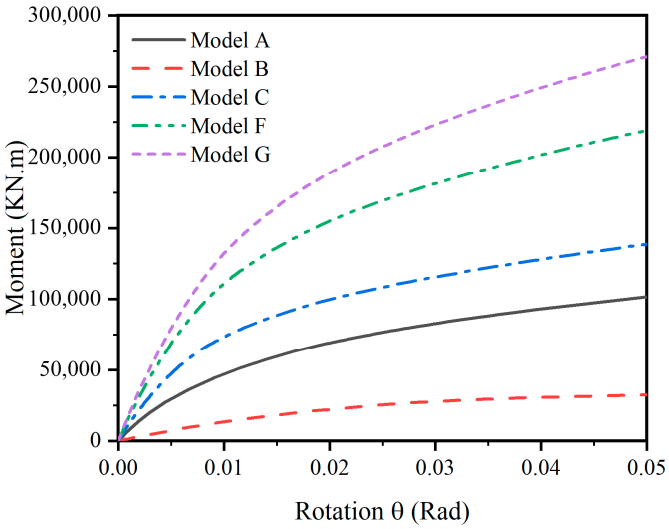
Figure 6. Lateral load–displacement responses of the pile–bucket foundation: (**a**) effect of bucket size, and (**b**) effect of loading eccentricity (*e*).

4.2. Ultimate Moment Capacity

Figure 7 shows the moment–rotation responses of pile–bucket foundations under different bucket sizes and loading eccentricities (*e*). To evaluate ultimate moment performance, lateral displacement was applied until the rotation reached approximately 0.05 rad. Beyond this rotation, the lateral load approached a plateau; hence, 0.05 rad was adopted as the criterion for ultimate moment capacity, consistent with lateral performance criteria reported in previous experimental and numerical studies [7,33].



(**a**)



(**b**)

Figure 7. Moment–rotation responses of the pile–bucket foundation: (**a**) effect of bucket size, and (**b**) effect of loading eccentricity (*e*).

Figure 7a compares the ultimate moment capacities of a single pile, a standalone bucket, and a pile–bucket system. The pile–bucket system exhibits significantly higher stiffness and moment capacity than both the single pile and the standalone bucket. The results further indicate that increasing the bucket diameter enhances both stiffness and moment capacity more effectively than increasing the bucket embedment depth. Figure 7b illustrates the influence of loading eccentricity on moment capacity. As the loading eccentricity increases, both stiffness and moment capacity decrease progressively.

4.3. Bearing Capacity Sharing Ratio

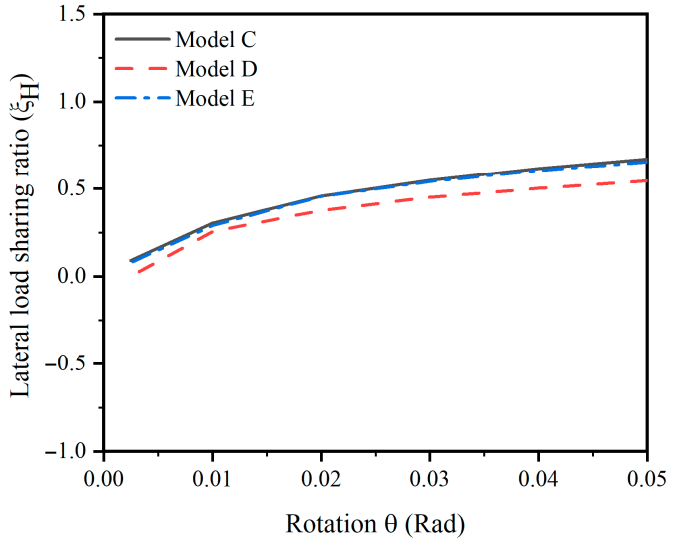
Based on previous studies that demonstrated the bearing capacity of the pile–bucket system, this section analyzes the individual contributions of the pile and the bucket through lateral load- and moment-sharing ratios [19,33].

$$\xi_H = \frac{H_P}{H} \quad (1)$$

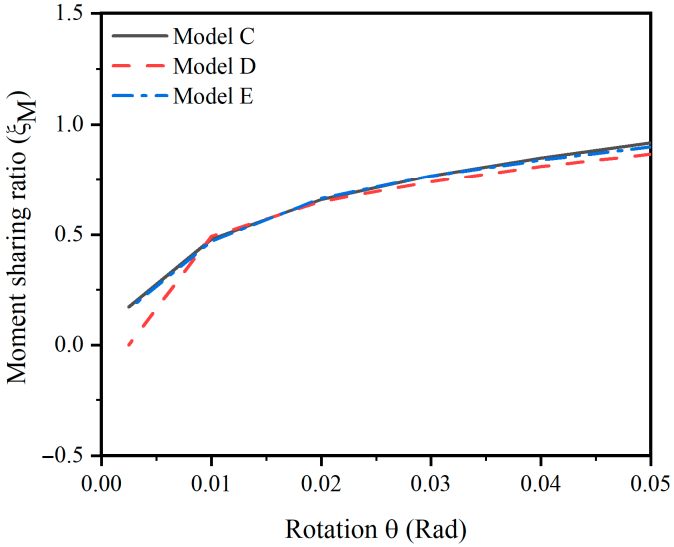
$$\xi_M = \frac{M_P}{M} \tag{2}$$

Here, H_P denotes the lateral load resisted by the single pile at the mudline, while H represents the total lateral load applied at the top of the pile–bucket foundation. Similarly, M_P corresponds to the moment sustained by the single pile at the mudline, and M is the moment induced at the mudline by the applied lateral load.

Figures 8 and 9 illustrate the evolution of load- and moment-sharing ratios under varying bucket sizes and loading eccentricities. With respect to bucket size, both the load- and moment-sharing ratios for the composite foundation decrease with increasing bucket diameter or embedment depth, with the effect more pronounced for larger diameters. These results indicate that increasing the bucket diameter contributes more to lateral resistance than increasing the embedment depth. At a rotation angle of 0.05 radians, the load-sharing ratio decreases significantly as loading eccentricity increases.



(**a**)



(**b**)

Figure 8. Effect of (**a**) the lateral load-sharing ratio; (**b**) the moment-sharing ratio with bucket size.

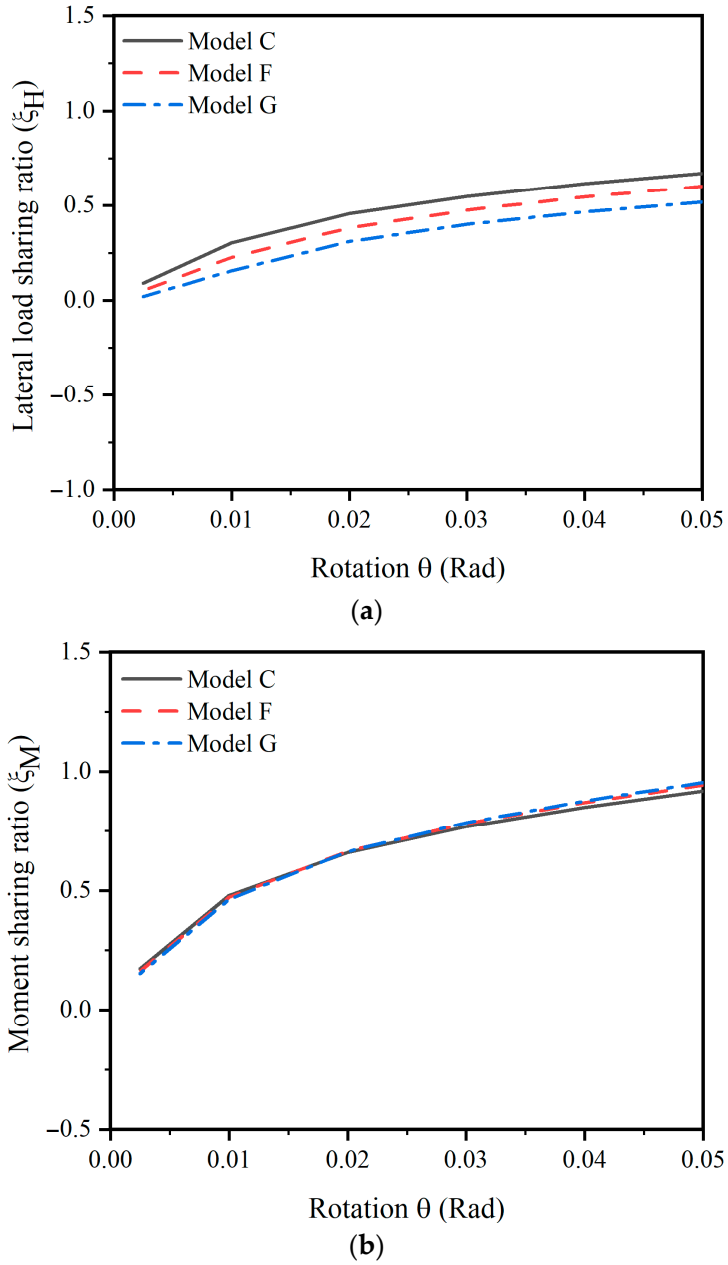


Figure 9. Effect of (**a**) the lateral load-sharing ratio; (**b**) the moment-sharing ratio with loading eccentricity.

At the mudline, the bucket carries the majority of the lateral load, reaching a maximum load-sharing ratio (ξ_H) of approximately 0.75. In contrast, the moment-sharing ratio (ξ_M) exhibits an opposite trend, with increasing loading eccentricity transferring a larger portion of the moment to the pile near the mudline. The moment-sharing ratio peaks at approximately 0.92, indicating that the pile resists the majority of the moment.

Overall, these results suggest that the single-pile functions as an anchoring element in the deeper soil, predominantly resisting moments, while the bucket distributes lateral loads within the shallow portion of the foundation, enhancing the overall load-bearing capacity compared with a single pile.

4.4. Rotation Center Position and Soil Failure Mechanism

The location of the rotation center is critical for assessing the lateral bearing capacity of single-pile foundations [46,47]. Figures 10 and 11 show the displacement contours

of the pile–soil system at a rotation angle of 0.05 rad, which is regarded as the onset of failure. These contours highlight the soil failure zone, providing clearer insight into the failure mechanisms of both single-pile and pile–bucket foundations subjected to lateral loading [48].

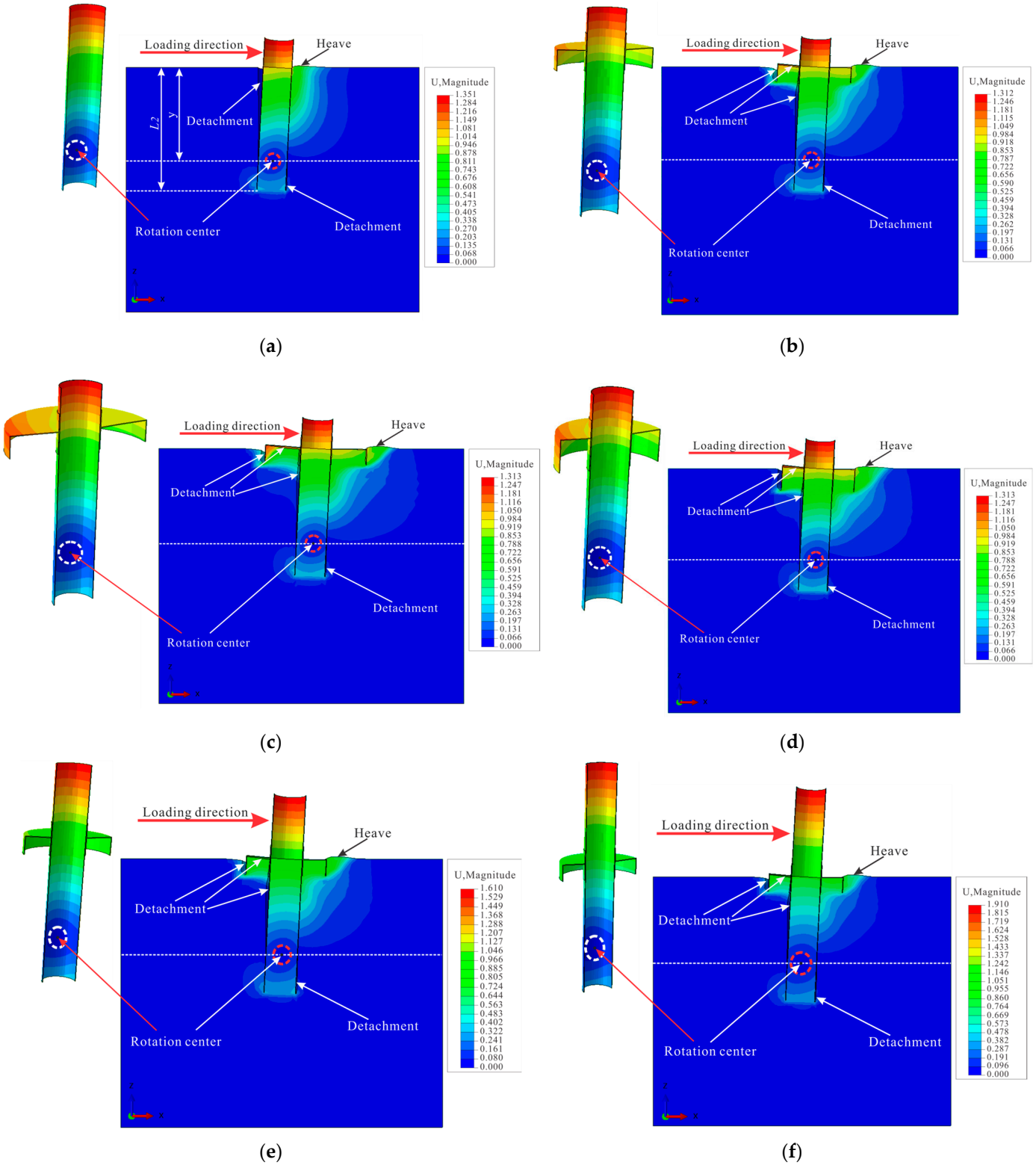


Figure 10. Displacement contours at a rotation angle of 0.05 rad for (**a**) Model A, (**b**) Model C, (**c**) Model D, (**d**) Model E, (**e**) Model F, and (**f**) Model G.

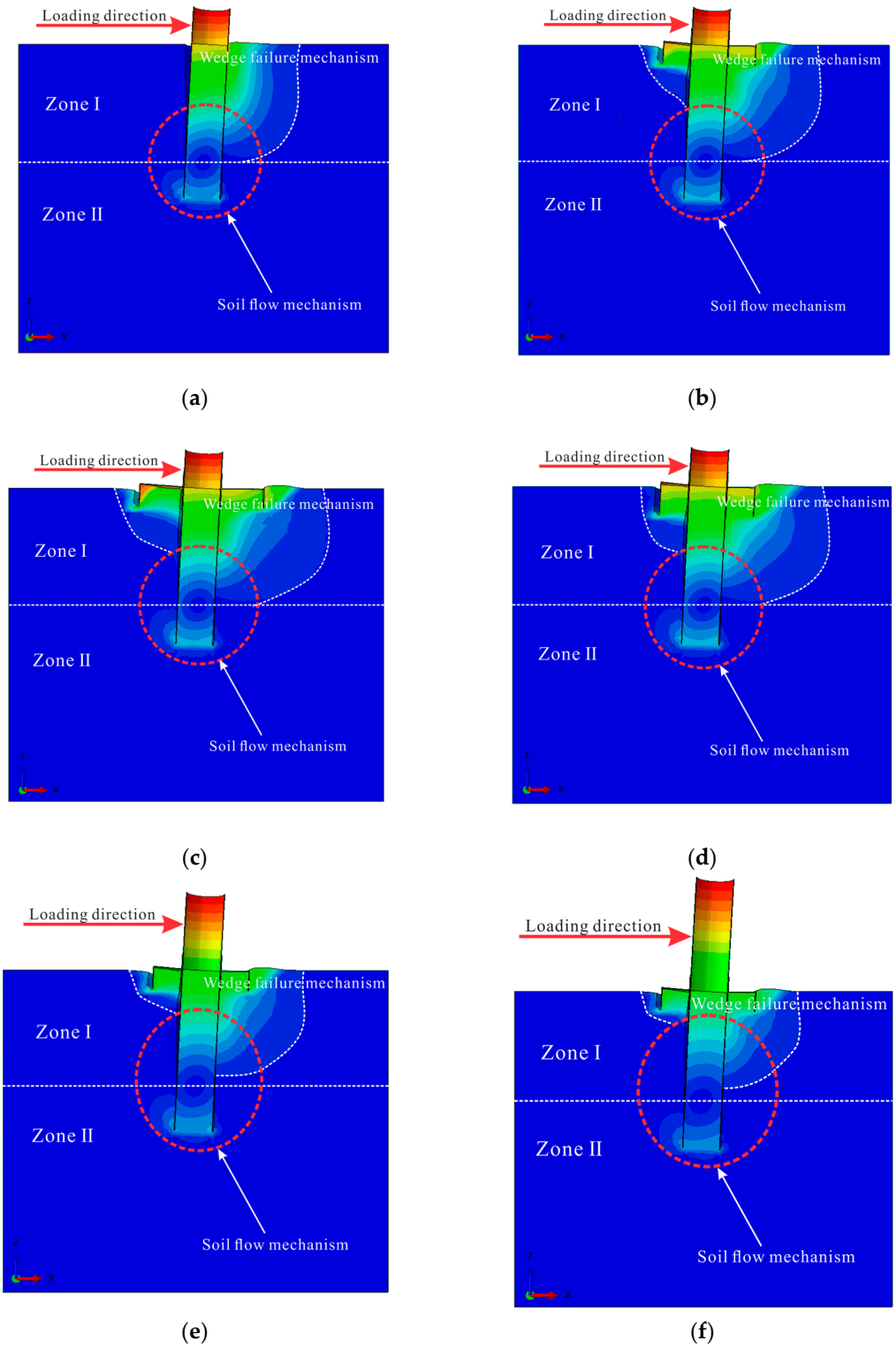


Figure 11. Soil flow mechanism around the single-pile and pile–bucket foundation (**a**) Model A, (**b**) Model C, (**c**) Model D, (**d**) Model E, (**e**) Model F, and (**f**) Model G.

In the examined cases, both single-pile and pile–bucket foundations exhibit a pronounced rotational failure mechanism, characterized by a well-defined rotation center near the pile base and soil detachment along the left side of the foundations. Soil detachment occurs beneath the bucket lid, along the skirt, and at the pile toe (Figure 10). For Models A, C, D, E, F, and G, two failure patterns were observed in the soil: wedge and rotational soil flow mechanisms (Figure 11). In the lower portion of both foundation types, circulating soil

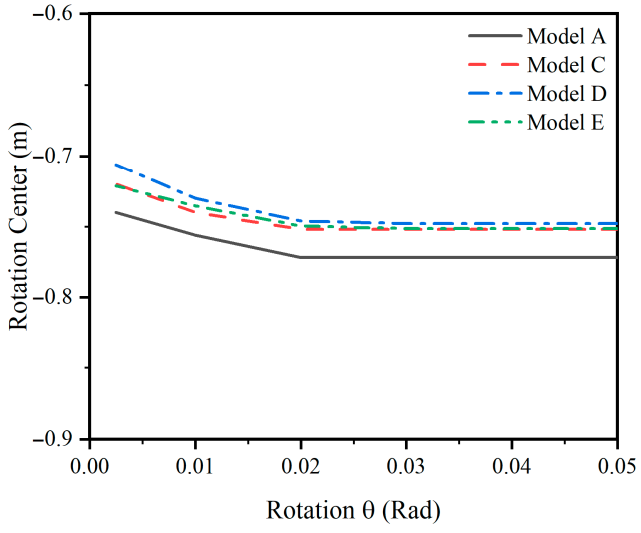
flow develops, followed by detachment of the pile on the right-hand side. This behavior aligns with the flow of soil around laterally loaded piles, where full flow behavior is not observed between the wedge and rotational zones [46,47]. In contrast, Model C shows that including a bucket elevates the rotation center and enlarges the rotating soil flow zone compared with Model A (single pile).

The results indicate that variations in bucket size have little effect on the soil failure mechanisms, as shown by comparisons among Models C, D, and E. However, Models D and E exhibit a larger wedge-shaped zone than Model C, suggesting more effective mobilization of soil resistance at shallow depths. Analysis of the rotational center shows that adding a shallow bucket does not fundamentally change the failure mechanism of a laterally loaded single pile, but it enlarges the surrounding soil flow region. These findings confirm the similarity of pile–soil interactions between single piles and pile–bucket foundations and provide guidance for designing the lateral bearing capacity of pile–bucket systems. Furthermore, adding a bucket enhances resistance from the shallow soil layers.

As loading eccentricity increases (Models C, F, and G), the rotation center moves upward. The rotational soil flow zone in Model G is larger than in Models C and F, with soil displacement occurring opposite to the applied lateral load. This behavior indicates that the lower portion of the pile develops a stronger reaction to resist the higher moment resulting from increased loading eccentricity.

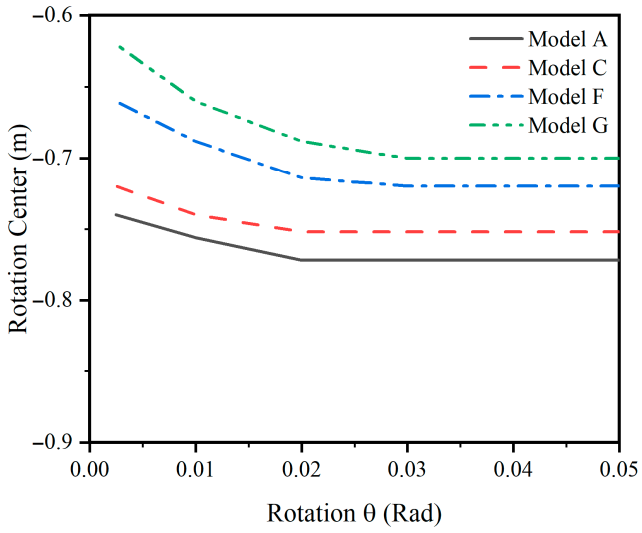
The rotation centers of both single-pile and pile–bucket foundations are generally located along the centerline, as shown in Figure 10. In stiff pile foundations, the depth of the rotation center influences the load transfer mechanism more significantly than lateral displacement [7,47]. Figure 12 presents the normalized depth, y/L_2, where L_2 is the embedment length and y is the rotation center depth. For direct comparison with the rotation center positions shown in Figure 10, the normalized depth is represented as a negative value.

The position of the rotation center shown in Figure 12a,b moves downward as the rotation angle increases. Comparison between the single-pile and pile–bucket foundations indicates that the inclusion of a bucket shifts the rotation center to a deeper position. Increases in loading eccentricity, bucket diameter, and embedment depth shift the rotation center upward by approximately 3–9% compared with a single pile, highlighting the influence of geometric configuration and loading conditions on rotation behavior.



(**a**)

Figure 12. *Cont.*



(**b**)

Figure 12. Variation in rotation center: (**a**) effect of bucket size, and (**b**) effect of loading eccentricity (e).

Figure 12a illustrates the influence of bucket size on variations in rotation center depth. Numerical results show that increasing bucket size has little effect during the early development stage, with Models C and E exhibiting nearly identical rotation center positions initially. At a rotation angle of 0.05 rad, Model D exhibits the deepest rotation center, followed by Model E, indicating that increasing bucket diameter enhances lateral resistance more effectively than increasing bucket embedment depth.

Figure 12b presents the effect of loading eccentricity (e) on rotation center depth. As the loading eccentricity increases from $1D_1$ to $3D_1$ (Models C, F, and G), the rotation center progressively moves deeper.

Determination of the Rotation Center Position and Soil Failure Mechanism

Li et al. [49] adopted the Winkler assumption to theoretically analyze the rotation center of an enhanced suction bucket foundation, which is analogous to the pile–bucket foundation. In their study, lateral and vertical soil pressure distributions were assumed to follow the Winkler model, while the effects of sidewall friction were also considered. The location of the rotation center was derived from mechanical equilibrium equations, as presented in Equation (3).

$$z_0 = \frac{\left(\frac{2}{3}I_0^3 - \frac{2}{3}I_1^3\right)r + \frac{2}{3}I_1^3 R}{I_1^2 R - r\left(I_1^2 - I_0^2\right)} \tag{3}$$

where z_0 is the depth of the rotation center beneath the mudline, I_0 and I_1 are the embedment depth of the pile and bucket, respectively, and r and R denote the radii of the pile and bucket.

Accordingly, the present study refines the rotation center formulation proposed by Li et al. [49] using results obtained from three-dimensional finite element analyses to improve the accuracy and applicability of rotation center prediction. This refinement facilitates more reliable stress analysis of pile–bucket foundations under lateral loading conditions and provides improved theoretical support for engineering applications. To maintain parameter consistency, Equation (3) is reformulated as follows:

$$z_0 = \frac{2\left(L_p^3 - L_b^3\right)d + L_b^3 D}{3L_p^2 D - d\left(L_b^2 - L_p^2\right)} \tag{4}$$

where L_P and L_b represent the embedment depths of the pile and bucket, respectively, while d and D denote the radii of the pile and bucket.

The rotation center positions obtained from finite element analysis were compared with those calculated using Equation (4) for Models A, B, and C to evaluate the effect of bucket size. The results are presented in Table 3. The comparison shows good agreement between the two methods, demonstrating consistent trends and a strong positive correlation. Statistical analysis yielded an average proportional coefficient of 1.16. Accordingly, a correction factor of 1.16 was introduced into the original formulation, resulting in a modified rotation center calculation applicable to pile–bucket foundations:

$$z_0 = 0.77\frac{\left(L_p^3 - L_b^3\right)d + L_b^3 D}{L_p^2 D - d\left(L_b^2 - L_p^2\right)} \tag{5}$$

Table 3. Comparison of rotation center positions.

Type	FEM	Theoretical Equation	Correction Factor
Model C	18.8	16.3566	1.149383124
Model D	18.7	16.1899	1.155041106
Model E	18.8	16.0333	1.17255961

Figure 13 compares the rotation depth y obtained from finite element simulations with theoretical predictions for Models C, D, and E. In all three cases, the rotation depths predicted numerically show close agreement with the theoretical results, indicating strong consistency between the analytical and numerical approaches. The variation among the models is relatively small, with rotation depths stabilizing at approximately 19 m.

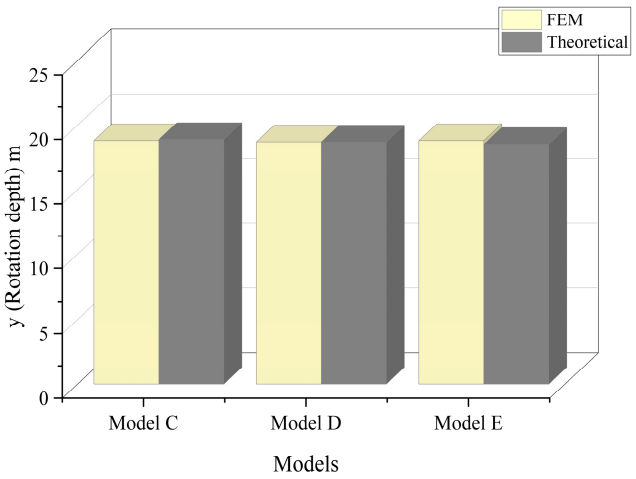


Figure 13. Compression of the rotation center depths calculated by FEM and theoretical methods for the pile–bucket foundation.

4.5. Static Bending Moment Profile

The bending moment generally increases with depth, as expected in deep foundations where both applied loads and soil resistance contribute to higher bending stresses. Figure 14 illustrates the influence of bucket size and loading eccentricity (e) on the bending moment distribution of pile–bucket foundations. As shown in Figure 14a, increasing the bucket diameter or embedment depth enhances bending moments, with embedment depth exerting a more pronounced effect, indicating that deeper soil engagement significantly improves moment resistance. Quantitatively, increasing bucket diameter or embedment depth raises bending moments by 5–9%, whereas higher loading eccentricity amplifies

bending moments by 32–50% relative to a single pile. Figure 14b highlights the impact of loading eccentricity, demonstrating that larger eccentricities amplify bending moments throughout the foundation, exceeding those observed in single-pile configurations. These results emphasize that the lateral load–moment response of pile–bucket foundations is strongly governed by both geometric parameters and load application point, providing critical insights for optimizing foundation design to mitigate excessive bending and improve overall structural performance.

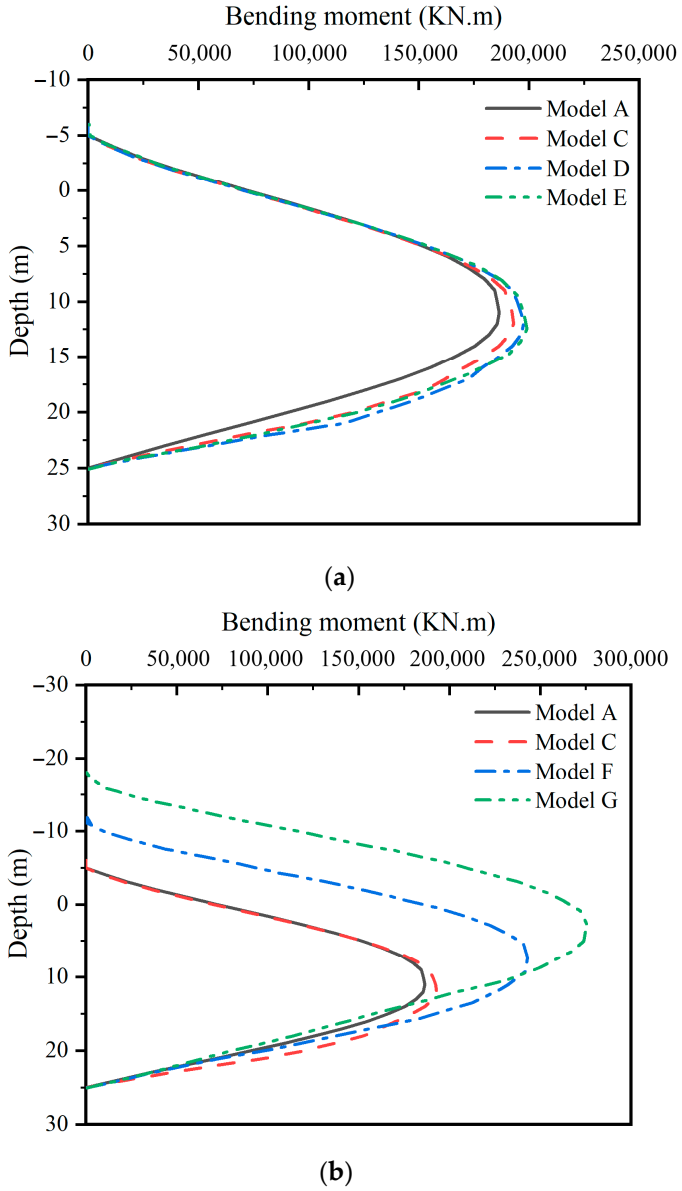


Figure 14. Bending moment distribution of the pile–bucket foundation. (**a**) Effect of bucket size, and (**b**) effect of load eccentricity (*e*).

5. Conclusions

This study conducted three-dimensional numerical analyses of single-pile and pile–bucket foundations to evaluate their lateral load capacity and failure mechanisms under displacement-controlled static loading. Based on the results, the following conclusions are drawn:

(1) The pile–bucket foundation exhibits superior initial stiffness and lateral load capacity compared with both single piles and standalone bucket foundations. The lateral

capacity increases by approximately 37–60% relative to a single pile and is 3–4 times greater than that of a standalone bucket. Increasing bucket diameter provides a more significant improvement than increasing embedment depth. However, increasing loading eccentricity reduces lateral capacity, shifting the response from an 8% improvement to a 10% reduction relative to the single-pile case. Larger bucket sizes and higher loading eccentricities also shift the rotation center upward.

(2) Load–moment-sharing analysis indicates that the bucket resists up to 75% of the lateral load at the mudline, while the pile carries up to 92% of the moment, demonstrating effective synergistic interaction between the two components. Increasing loading eccentricity reduces lateral load sharing by the bucket and increases moment transfer to the pile.

(3) Both single-pile and pile–bucket foundations exhibit rotation-dominated failure under static lateral loading. The soil failure mechanism is characterized by wedge-type failure near the mudline and rotational soil flow at depth. The bucket does not alter the fundamental failure mode but enlarges the soil deformation zone.

(4) Integration of the bucket and increased loading eccentricity cause an upward shift in the rotation center, enhancing soil resistance along the lower portion of the pile. The rotation center stabilizes at approximately 19 m depth, with larger bucket dimensions or higher eccentricity producing further upward movement. Overall, increases in loading eccentricity, bucket diameter, and embedment depth shift the rotation center upward by approximately 3–9% compared with a single pile.

(5) Bending moments increase with foundation size and loading eccentricity. Increasing bucket diameter or embedment depth raises bending moments by 5–9%, while higher eccentricity amplifies them by 32–50% relative to a single pile.

(6) A modified analytical expression for predicting the rotation center position is proposed, incorporating a correction factor of 1.16 to improve the accuracy of design calculations for pile–bucket foundations.

It should be noted that the present study is based on three-dimensional finite element simulations using the Mohr–Coulomb constitutive model and assumes homogeneous silty sand under static lateral loading. The proposed correction factor 1.16 was calibrated within the investigated bucket diameter and embedment depth range. Therefore, their applicability to different soil conditions (e.g., soft clay), cyclic or dynamic loading, and substantially different foundation configurations requires further validation. Future research incorporating advanced constitutive models and experimental verification is recommended to enhance the generalization of the findings.

Author Contributions: Conceptualization, M.A.F., W.W., M.A.A. and J.Y.; methodology, M.A.F., M.X. and W.W.; Software, M.A.F. and R.L.; formal analysis, M.A.F., M.X., L.L., T.I., C.W. and R.L., Data curation, M.X., L.L., T.I. and C.W.; writing—original draft preparation, M.A.F.; writing—review and editing, L.L., W.W., M.A.A. and J.Y.; supervision, W.W.; project administration, W.W.; funding acquisition, W.W. All authors have read and agreed to the published version of the manuscript.

Funding: This research is supported by the National Natural Science Foundation of China (Grant Nos. 52178371, 52168046, 52578446 and 52538008), the 'CUG Scholar' Scientific Research Funds at China University of Geosciences (Wuhan) (Project No. 2023121), Guangdong Basic and Applied Basic Research Foundation (2024A1515240075), the Research Project of Engineering Research Centre of Rock–Soil Drilling & Excavation and Protection, Ministry of Education (Grant No. 202305), and the Guangdong Basic and Applied Basic Research Foundation (Grant No. 2023A1515240012).

Data Availability Statement: Data is available on request from the authors.

Conflicts of Interest: Authors Jingliang Ye, Chunbin Wan and Ruqin Luo were employed by the company Wuhan Yucheng Construction Group Co., Ltd. The remaining authors declare that the

research was conducted in the absence of any commercial or financial relationships that could be construed as a potential conflict of interest.

References

1. Randolph, M.; Gourvenec, S. *Offshore Geotechnical Engineering*; CRC Press: Boca Raton, FL, USA, 2017.
2. Lehane, B.M.; Powrie, W.; Doherty, J.P. Centrifuge model tests on piled footings in clay for offshore wind turbines. In *Frontiers in offshore geotechnics II*; CRC Press: Boca Raton, FL, USA, 2010; pp. 623–628.
3. Lehane, B.M.; Pedram, B.; Doherty, J.A.; Powrie, W. Improved performance of monopiles when combined with footings for tower foundations in sand. *J. Geotech. Geoenviron. Eng.* **2014**, *140*, 04014027. [CrossRef]
4. Anastasopoulos, I.; Theofilou, M. Hybrid foundation for offshore wind turbines: Environmental and seismic loading. *Soil Dyn. Earthq. Eng.* **2016**, *80*, 192–209. [CrossRef]
5. Wu, W.B.; Lu, C.H.; Chen, L.B.; Mei, G.X.; El Naggar, M.H.; Liu, H. Horizontal vibration characteristics of pile groups in unsaturated soil considering coupled pile–pile interaction. *Ocean Eng.* **2023**, *281*, 115000. [CrossRef]
6. Byrne, B.; Houlsby, G.; Martin, C.; Fish, P. Suction caisson foundations for offshore wind turbines. *Wind. Eng.* **2002**, *26*, 145–155. [CrossRef]
7. LeBlanc, C.; Houlsby, G.T.; Byrne, B.W. Response of stiff piles in sand to long-term cyclic lateral loading. *Géotechnique* **2010**, *60*, 79–90. [CrossRef]
8. Liao, Y.D.; Guo, M.Y.; Wang, N.; Hou, L.J.; Chen, D. Dynamic responses of K-type and inverted-K-type jacket support structures for offshore wind turbines. *J. Cent. S. Univ.* **2017**, *24*, 947–956.
9. Zhou, X.; Lu, D.C.; Du, X.L.; Wang, G.S.; Meng, F.P. A 3D non-orthogonal plastic damage model for concrete. *Comput. Methods Appl. Mech. Eng.* **2020**, *360*, 112716. [CrossRef]
10. Zaaijer, M.B. Foundation modelling to assess dynamic behaviour of offshore wind turbines. *Appl. Ocean Res.* **2006**, *28*, 45–57. [CrossRef]
11. Chen, D.; Huang, K.; Bretel, V.; Hou, L. Comparison of structural properties between monopile and tripod offshore wind-turbine support structures. *Adv. Mech. Eng.* **2013**, *5*, 175684. [CrossRef]
12. Myhr, A.; Bjerkseter, C.; Ågotnes, A.; Nygaard, T.A. Levelised cost of energy for offshore floating wind turbines in a life cycle perspective. *Renew. Energy* **2014**, *66*, 714–728. [CrossRef]
13. Wang, X.; Zeng, X.; Li, J.; Yang, X. Lateral bearing capacity of hybrid monopile–friction wheel foundation for offshore wind turbines by centrifuge modelling. *Ocean Eng.* **2018**, *148*, 182–192.
14. Qu, X.Q.; Wang, R.; Zhang, J.M.; He, B. Influence of soil plug on the seismic response of bucket foundations in liquefiable seabed. *J. Mar. Sci. Eng.* **2023**, *11*, 598. [CrossRef]
15. Liu, X.; Wu, W.B.; El Naggar, M.H.; Sun, J.; Tang, L. Theoretical analysis of dynamic performance of concrete-filled steel tube pile under vertical load. *Comput. Geotech.* **2024**, *165*, 105884.
16. Wang, X.; Li, S.; Li, J. Load bearing mechanism and simplified design method of hybrid monopile foundation for offshore wind turbines. *Appl. Ocean Res.* **2022**, *126*, 103286. [CrossRef]
17. Lu, D.C.; Wang, G.S.; Du, X.L.; Wang, Y. A nonlinear dynamic uniaxial strength criterion that considers the ultimate dynamic strength of concrete. *Int. J. Impact Eng.* **2017**, *103*, 124–137. [CrossRef]
18. He, B.; Yuan, Z.Y.; Jiang, Z.Q.; Ni, D.Y.; Shi, L.; Yuan, Z.H.; Sun, H.L. Model tests on horizontal load-bearing and deformation resistance capacities of pile-bucket foundation in soft seabed soil. *Mar. Georesour. Geotechnol.* **2022**, *40*, 1193–1204. [CrossRef]
19. Shi, L.; Yuan, Z.; Yuan, Z.; Sun, H.; Cai, Y. On load-bearing and soil-reacting characteristics of hybrid pile-bucket foundations subjected to static horizontal loading. *Mar. Struct.* **2022**, *84*, 103222.
20. Li, D.; Lin, Z.; Wu, Y.; Zhang, Y.; Li, S. Lateral ultimate bearing capacity of modified suction caisson in uniform and linearly increasing strength undrained clays. *Int. J. Numer. Anal. Methods Geomech.* **2023**, *47*, 2085–2095.
21. Liu, R.; Shi, J.; Chen, G.; Yang, X. Lateral bearing capacity and calculation method of pile-bucket foundation in clay for offshore wind turbines. *Ocean Eng.* **2023**, *283*, 115039. [CrossRef]
22. Bienen, B.; Gaudin, C.; Cassidy, M.J.; Rausch, L.; Purwana, O.A.; Krisdani, H. Numerical modelling of a hybrid skirted foundation under combined loading. *Comput. Geotech.* **2012**, *45*, 127–139. [CrossRef]
23. Fu, Z.; Wang, G.; Yu, Y.; Shi, L. Model test study on bearing capacity and deformation characteristics of symmetric pile–bucket foundation subjected to cyclic horizontal load. *Symmetry* **2021**, *13*, 1647. [CrossRef]
24. Wang, X.; Zeng, X.; Li, X.; Li, J. Investigation on offshore wind turbine with an innovative hybrid monopile foundation: An experimental-based study. *Renew. Energy* **2019**, *132*, 129–141. [CrossRef]
25. Lu, D.C.; Meng, F.P.; Zhou, X.; Zhuo, Y.H.; Gao, Z.W.; Du, X.L. A dynamic elastoplastic model of concrete based on a modeling method with environmental factors as constitutive variables. *J. Eng. Mech.* **2023**, *149*, 04023102. [CrossRef]
26. Chen, W.; Jiang, Y.; Xu, L.; Liu, C.; Chen, G.; Wang, P. Seismic response of hybrid pile-bucket foundation supported offshore wind turbines located in liquefiable soils. *Ocean Eng.* **2023**, *269*, 113519. [CrossRef]

27. Li, X.; Zhang, M. Soil–structure interaction of a laterally loaded hybrid foundation for offshore wind turbine. *Ocean Eng.* **2022**, *263*, 112197. [CrossRef]
28. Chen, W.Y.; Jiang, Y.J.; Huang, L.C.; Xu, L.Y.; Liu, C.; Chen, G.X. Nonlinear seismic performance of offshore wind turbines on hybrid pile-bucket foundation in sand. *Soil. Dyn. Earthq. Eng.* **2024**, *187*, 108981. [CrossRef]
29. Li, L.C.; Yan, N.X.; Liu, Z.; Wu, W.B.; Jiang, G.S.; Chen, L.B.; Liu, H. Investigation on the cyclic laterally-loaded response of pile-bucket foundation with grouted connection. *Mar. Struct.* **2025**, *103*, 103808. [CrossRef]
30. Li, L.C.; Wu, W.B.; Jiang, G.S.; El Naggar, M.H.; Liu, X.; Liao, K.; Liu, H. Discrete-continuum modelling on the bearing mechanism of pile-bucket foundation under static lateral load. *Ocean Eng.* **2025**, *318*, 120149. [CrossRef]
31. Li, L.C.; Liu, H.; Jiang, G.S.; Liu, Z.; El Naggar, M.H.; Wu, W.B. Numerical analysis on the mechanical response of grouted connection for pile-bucket foundation. *Ocean Eng.* **2023**, *287*, 115790. [CrossRef]
32. Ma, C.; Lu, D.C.; Du, X.L.; Qi, C.Z.; Zhang, X.Y. Structural components functionalities and failure mechanism of rectangular underground structures during earthquakes. *Soil Dyn. Earthq. Eng.* **2019**, *119*, 265–280. [CrossRef]
33. Chen, D.; Gao, P.; Huang, S.; Li, C.; Yu, X. Static and dynamic loading behavior of a hybrid foundation for offshore wind turbines. *Mar. Struct.* **2020**, *71*, 102727. [CrossRef]
34. Pan, X.; He, B.; Yuan, Z.; Xu, S.; Xu, D.; Jiang, Z.; Shi, L.; Sun, H. Effect of reinforced bucket on bearing capacity and natural frequency of offshore wind turbines using pile–bucket foundation. *Adv. Civ. Eng.* **2022**, *2022*, 9569102. [CrossRef]
35. Arshi, H.S.; Stone, K.J.L. Lateral resistance of hybrid monopile-footing foundations in cohesionless soils for offshore wind turbines. In *SUT Offshore Site Investigation and Geotechnics*; SUT: London, UK, 2012.
36. Ma, H.; Yang, J. A novel hybrid monopile foundation for offshore wind turbines. *Ocean Eng.* **2020**, *198*, 106963. [CrossRef]
37. Wang, B.; Qin, T.; Yuan, C.; Li, L.; Yuan, M.; Li, Y. Analysis of bearing performance of monopile and single suction bucket foundation for offshore wind power under horizontal load. *Geofluids* **2022**, *2022*, 4163240. [CrossRef]
38. Liu, W.B.; Zhao, L.; Jia, N. Numerical simulation of bearing capacity of pile-bucket foundation under combined loading of uplift and horizontal force. *Adv. Mater. Res.* **2011**, *243*, 2171–2175.
39. Zhang, X.; Yu, D.; Zhu, K.; Zhao, A.; Ren, M. Horizontal bearing characteristics and microscopic soil deformation mechanism of pile-bucket composite foundation in sand. *Appl. Sci.* **2024**, *14*, 907. [CrossRef]
40. Fan, M.; Duan, L.; Wang, D.; Zhan, B.; Shen, L. Experimental study on mechanical behavior of skirt–pile foundations in saturated clay under horizontal load. *Appl. Sci.* **2024**, *14*, 3345. [CrossRef]
41. Li, L.C.; Zheng, M.Y.; Liu, X.; Wu, W.B.; Liu, H.; El Naggar, M.H.; Jiang, G.S. Numerical analysis of the cyclic loading behavior of monopile and hybrid pile foundation. *Comput. Geotech.* **2022**, *144*, 104635. [CrossRef]
42. Dassault Systèmes. *Abaqus 2022: Standard/Explicit, User's Manual*; Dassault Systemes: Vélizy-Villacoublay, France, 2022. Available online: https://www.3ds.com/products-services/simulia/products/abaqus/ (accessed on 28 February 2026).
43. Lai, Y.; Li, W.; He, B.; Wang, L.; Xiong, G.; Liu, T. Centrifuge modelling of monotonic and cyclic lateral responses of a hybrid monopile-bucket foundation for offshore wind turbines. *Ocean Eng.* **2022**, *260*, 111967. [CrossRef]
44. Çetindemir, O. A review of modeling issues on the seismic soil-pile-structure interaction. *KSCE J. Civ. Eng.* **2024**, *28*, 3359–3377. [CrossRef]
45. Li, D.; Zhang, Y.; Feng, L.; Gao, Y. Capacity of modified suction caissons in marine sand under static horizontal loading. *Ocean Eng.* **2015**, *102*, 1–16. [CrossRef]
46. Hong, Y.; He, B.; Wang, L.Z.; Wang, Z.; Ng, C.W.W.; Mašín, D. Cyclic lateral response and failure mechanisms of semi-rigid pile in soft clay. *Can. Geotech. J.* **2017**, *54*, 806–824. [CrossRef]
47. Wang, H.; Lehane, B.M.; Bransby, M.F.; Wang, L.Z.; Hong, Y.; Askarinejad, A. Lateral behavior of monopiles in sand under monotonic loading. *Ocean Eng.* **2023**, *277*, 114334. [CrossRef]
48. Otani, J.; Pham, K.D.; Sano, J. Investigation of failure patterns in sand due to laterally loaded pile using X-ray CT. *Soils Found.* **2006**, *46*, 529–535. [CrossRef]
49. Li, D.Y.; Ma, S.L.; Zhang, Y.K.; Chen, F.Q. Lateral bearing capacity of modified suction caissons determined using the limit equilibrium method. *China Ocean Eng.* **2018**, *32*, 461–466. [CrossRef]

Disclaimer/Publisher's Note: The statements, opinions and data contained in all publications are solely those of the individual author(s) and contributor(s) and not of MDPI and/or the editor(s). MDPI and/or the editor(s) disclaim responsibility for any injury to people or property resulting from any ideas, methods, instructions or products referred to in the content.